

# Tunable Light–Matter Interaction and the Role of Hyperbolicity in Graphene–hBN System

Anshuman Kumar,<sup>†</sup> Tony Low,<sup>‡,§</sup> Kin Hung Fung,<sup>¶</sup> Phaedon Avouris,<sup>‡</sup> and Nicholas X. Fang\*,<sup>†</sup>

<sup>†</sup>Mechanical Engineering Department, Massachusetts Institute of Technology, Cambridge, Massachusetts 02139, United States

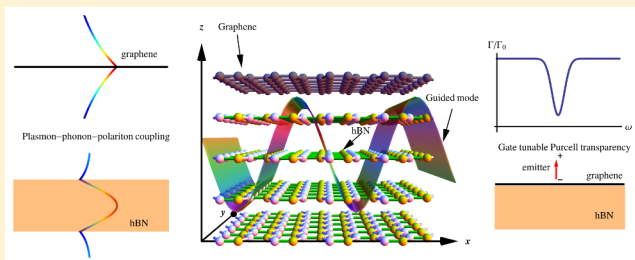
<sup>‡</sup>IBM T.J. Watson Research Center, 1101 Kitchawan Road, Yorktown Heights, New York 10598, United States

<sup>¶</sup>Department of Applied Physics, The Hong Kong Polytechnic University, Hong Kong, China

<sup>§</sup>Department of Electrical & Computer Engineering, University of Minnesota, Minneapolis, Minnesota 55455, United States

## S Supporting Information

**ABSTRACT:** Hexagonal boron nitride (hBN) is a natural hyperbolic material, which can also accommodate highly dispersive surface phonon-polariton modes. In this paper, we examine theoretically the mid-infrared optical properties of graphene–hBN heterostructures derived from their coupled plasmon–phonon modes. We find that the graphene plasmon couples differently with the phonons of the two Reststrahlen bands, owing to their different hyperbolicity. This also leads to distinctively different interaction between an external quantum emitter and the plasmon–phonon modes in the two bands, leading to substantial modification of its spectrum. The coupling to graphene plasmons allows for additional gate tunability in the Purcell factor and narrow dips in its emission spectra.



**KEYWORDS:** Plasmonics, graphene, hyperbolic metamaterials, hBN, phonons

Polaritons are hybrid modes of photons and charge dipole carrying excitations in crystals. Two of the most common types are surface plasmon polaritons<sup>1–3</sup> and phonon polaritons.<sup>4–10</sup> Such modes have been shown to be of technological relevance in subwavelength imaging,<sup>11,12</sup> biosensing,<sup>13,14</sup> waveguiding,<sup>2,15</sup> photovoltaics,<sup>16</sup> and quantum information.<sup>17–19</sup> While surface plasmons rely on free electron oscillations, surface phonons exist because of the lattice vibrations in polar crystals.<sup>20–23</sup>

Graphene has been shown to be a good candidate for tunable plasmonics in the mid-infrared (IR) and terahertz range,<sup>19,24–28</sup> owing to the possibility of electrostatic doping<sup>29</sup> and its ability to produce higher confinement and lower losses compared to metals.<sup>30</sup> On the other hand, near-field imaging has shown that phonon polaritons in hexagonal boron nitride (hBN) possess extremely high confinement and even lower loss compared to graphene plasmon polaritons.<sup>5</sup> hBN shows natural hyperbolicity,<sup>10</sup> which can potentially be used to explore exotic photonic properties<sup>31</sup> such as strong spontaneous emission enhancement,<sup>32,33</sup> negative refraction,<sup>34</sup> and thermal radiation enhancement.<sup>35</sup> Since both graphene plasmons and hBN phonons reside in the mid-IR, the optical properties of graphene–hBN heterostructures would allow one to marry the advantage of their constituents, electrical tunability in the former and high quality factor of the latter, through their hybrid plasmon–phonon polaritons.

The study of the optical properties of graphene–hBN heterostructures is also motivated by the following recent developments. First, hBN is now being used as a substrate of

choice for graphene due to the preservation of high carrier mobility, as opposed to conventional SiO<sub>2</sub> substrates.<sup>36</sup> The higher carrier mobility also translates to better plasmon quality factors.<sup>37</sup> Second, phonon modes of hBN can couple to graphene plasmon providing the possibility of observing interesting effects such as phonon-induced transparency.<sup>38</sup> Recently, a study of patterned graphene on monolayer hBN revealed a coherent coupling between plasmon modes in graphene and optical phonon modes in single-layer hBN.<sup>39</sup> As shown in ref 5, hBN thin films can support several higher order phonon-polaritonic waveguide modes inside the Reststrahlen band. These modes show a dispersion, which can be efficiently controlled by varying the thickness of the slab. Moreover, in the context of 3D resonators, highly confined hyperbolic phonon polaritons in hBN nanocones were reported recently.<sup>6</sup> In addition, both graphene and hBN can be grown in large area using chemical vapor deposition (CVD) techniques,<sup>40,41</sup> hence allowing in principle the construction of arbitrary heterostructures multilayers stack. The combination of these properties render graphene–hBN heterostructure an interesting photonic system.

Typical configuration of the graphene–hBN heterostructure studied in this work, that is, monolayer graphene deposited on hBN thin film, is shown in Figure 1, panel a. First, we will

**Received:** January 23, 2015

**Revised:** April 16, 2015

**Published:** April 21, 2015

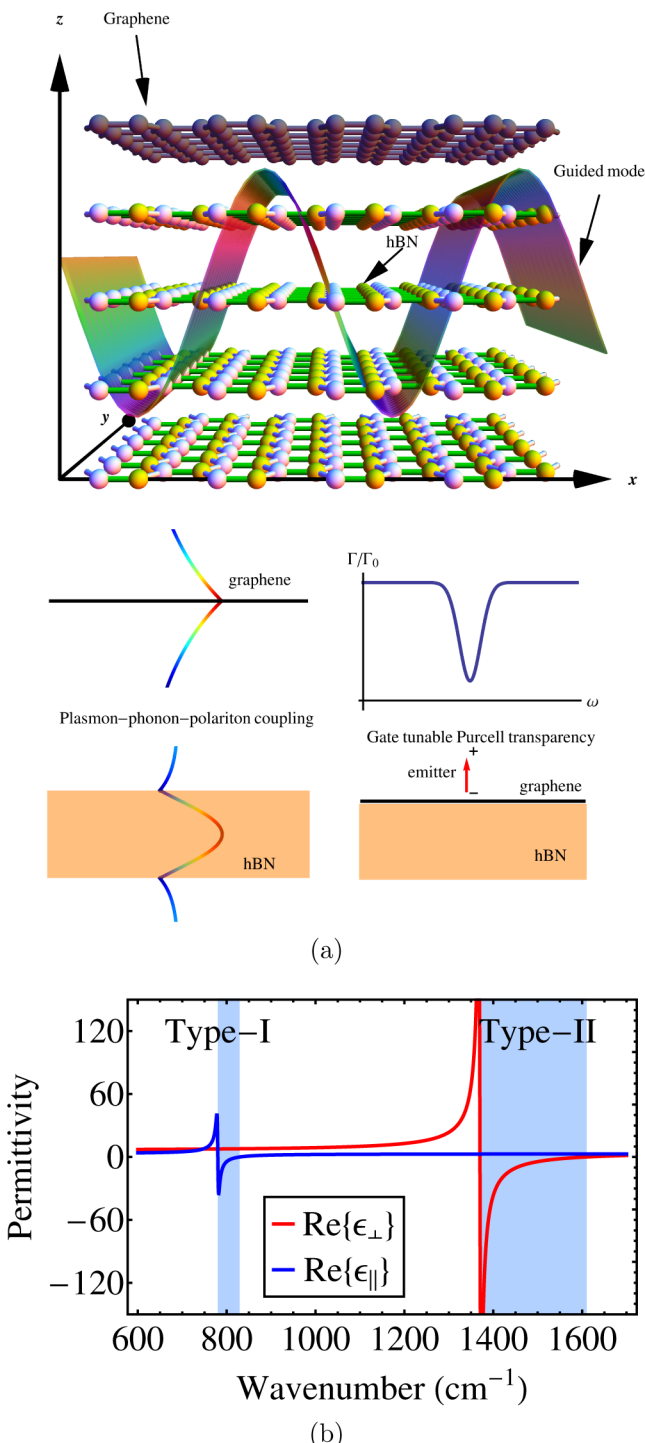


**Figure 1.** (a) Illustration of the problem. Monolayer graphene deposited on hBN film of thickness  $t_{\text{hBN}}$ . The figure is not to scale. This work focuses on the interaction of graphene plasmon with phonon in hBN (left) and the emission of a nearby dipole into these hybrid modes (right). (b) Permittivity tensor components of hBN clearly show the possibility of hyperbolicity in certain frequency ranges. The relevant parameters for the phonon frequencies were obtained from a previous study.<sup>42</sup>

describe the nature of the couplings between graphene plasmons and phonons of hBN for two different regimes of the hyperbolicity of hBN. Second, we exploit this coupling to demonstrate the possibility of inducing a dip in the Purcell spectrum due to this plasmon-phonon coupling and show its

tunability via the external knobs of hBN slab thickness and of active tuning using electrostatic gating.

**Optical Response of hBN and Graphene. Hexagonal Boron Nitride.** Hyperbolic materials are anisotropic materials where the relative permittivity tensor is such that one of the three components has a sign different from that of the other two. This property leads to a hyperbolic or indefinite dispersion for electromagnetic waves propagating inside such a material, which results in exotic photonic properties.<sup>31</sup> Until recently, most practical realizations of hyperbolic media relied on artificially engineered systems or the so-called metamaterials. However, the recent discovery of natural hyperbolicity in hBN crystals<sup>5</sup> would make possible the design of atomic scale hyperbolic metamaterials and might potentially allow one to cross over to regimes beyond the simple effective medium description in conventional hyperbolic metamaterials.

hBN is a van der Waals crystal with two kinds of IR active phonon modes relevant to hyperbolicity: (1) out-of-plane  $A_{2u}$  phonon modes, which have  $\omega_{\text{TO}} = 780 \text{ cm}^{-1}$ ,  $\omega_{\text{LO}} = 830 \text{ cm}^{-1}$ ; and (2) in-plane  $E_{1u}$  phonon modes, which have  $\omega_{\text{TO}} = 1370 \text{ cm}^{-1}$ ,  $\omega_{\text{LO}} = 1610 \text{ cm}^{-1}$ .<sup>42</sup> This leads to two distinct Reststrahlen (RS) bands, where the lower frequency RS band corresponds to type-I hyperbolicity ( $\epsilon_{\parallel} < 0$ ,  $\epsilon_{\perp} > 0$ ), and the upper RS band shows type-II hyperbolicity ( $\epsilon_{\perp} < 0$ ,  $\epsilon_{\parallel} > 0$ ). The hBN permittivity is given by

$$\epsilon_m = \epsilon_{\infty,m} + \epsilon_{\infty,m} \times \frac{(\omega_{\text{LO},m})^2 - (\omega_{\text{TO},m})^2}{(\omega_{\text{TO},m})^2 - \omega^2 - i\omega\Gamma_m} \quad (1)$$

where  $m = \perp, \parallel$ . The parameters employed in the above equation are taken from ref 42. In addition to the LO and TO frequencies, which have been mentioned in the previous paragraph, the other parameters are  $\epsilon_{\infty,\perp} = 4.87$ ,  $\epsilon_{\infty,\parallel} = 2.95$ ,  $\Gamma_{\perp} = 5 \text{ cm}^{-1}$ , and  $\Gamma_{\parallel} = 4 \text{ cm}^{-1}$ .

**Graphene.** The graphene response is modeled using local random phase approximation (local RPA). At temperature  $T$ , the 2D conductivity of graphene is given by<sup>43</sup>

$$\sigma_{\text{RPA}}(\omega) = \frac{2e^2kT}{\pi\hbar^2} \frac{i}{\omega + i/\tau} \ln \left[ 2 \cosh \left( \frac{\mu}{2kT} \right) \right] + \frac{e^2}{4\hbar} \left[ H(\omega/2, T) + \frac{4i\omega}{\pi} \int_0^\infty d\xi \frac{H(\xi, T) - H(\omega/2, T)}{\omega^2 - 4\xi^2} \right] \quad (2)$$

where  $H(\omega, T) = \sinh(\hbar\omega/kT)/[\cosh(\mu/kT) + \cosh(\hbar\omega/kT)]$ . The first term in eq 2 represents intraband contribution, and the remaining terms are contributions of the interband transitions to the total graphene conductivity. Here,  $\tau$  is the electron relaxation time. While Landau damping itself is already included in the conductivity model, the relaxation time typically has other contributions from (1) impurity scattering, (2) scattering with phonons ( $\hbar\omega_{\text{OPh}} = 0.2 \text{ eV}$ ) in graphene and phonon modes of polar substrates, (3) higher-order processes such as phonon coupled to  $e$ - $h$  excitations (which have to be treated separately), etc.<sup>27,37,44</sup> In literature, relaxation times as long as 1000 fs have been reported.<sup>36,45</sup> However, for frequencies larger than the optical phonon frequency of graphene, typically  $\tau \approx 50 \text{ fs}$ .<sup>27</sup> In this work, we use a graphene DC mobility  $\mu_{\text{DC}} = 10,000 \text{ cm}^2 \text{ V}^{-1} \text{ s}^{-1}$ . The mobility and relaxation time are related by  $\tau = \mu_{\text{DC}} E_F / eV_F$ .<sup>2,30</sup> The relaxation times considered in this work are in the same order of magnitude range as in ref 37.

**Plasmon-Phonons: Two Regimes of Mode Coupling.** We consider the geometry as shown in Figure 1, panel a. In this

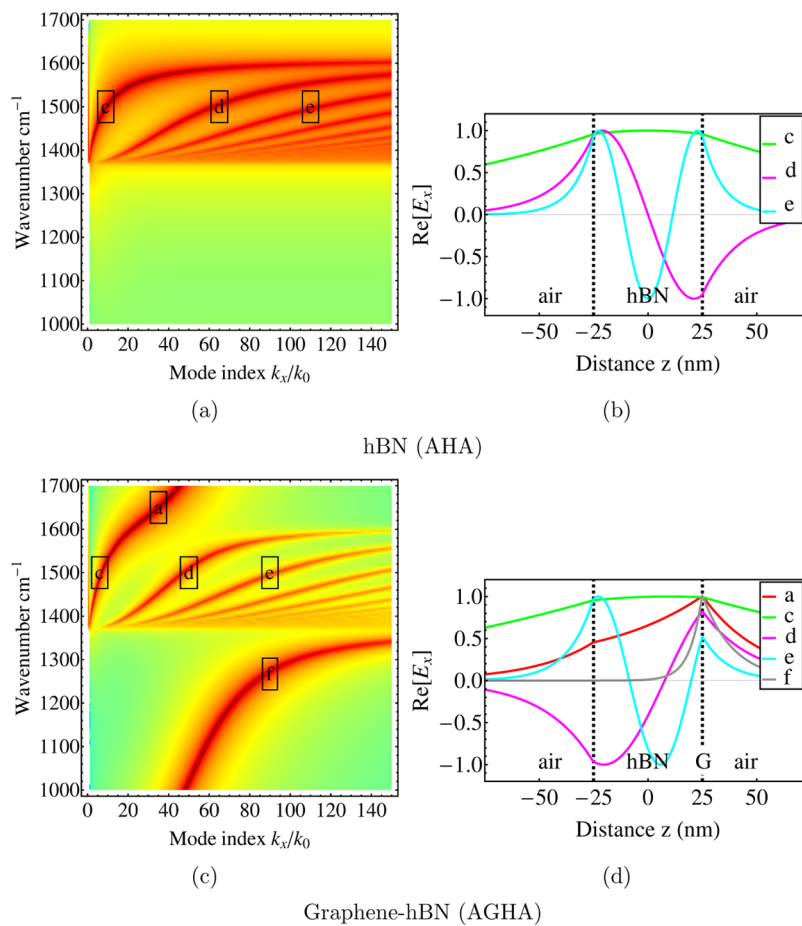


**Figure 2.** Dispersion curves and mode profiles for phonon polaritons in hBN thin slab (AHA) and coupled phonon–plasmon-polariton modes in graphene–hBN system (AGHA) near the in-plane (upper) RS band. Panels a–d represent the dispersion and mode profiles near the in-plane (upper) resonance of hBN. The alphabetical labels at different  $(k_x, \omega)$  points on each of the dispersion diagrams correspond to the field profiles on their immediate right. Thickness of hBN is  $t_{\text{hBN}} = 50$  nm, and graphene Fermi level is assumed to be 0.5 eV. Here, AHA and AGHA denote air–hBN–air and air–graphene–hBN–air, respectively.

general case, by invoking the quasistatic approximation, the modal dispersion inside the two RS bands can be written as

$$q(\omega) = -\frac{\psi}{t_{\text{hBN}}} \left[ \tan^{-1} \left\{ \frac{\epsilon_a + i(q/k_0)Z_0\sigma}{\epsilon_{\perp}\psi} \right\} + \tan^{-1} \left\{ \frac{\epsilon_s}{\epsilon_{\perp}\psi} \right\} + \pi n \right] \quad (3)$$

where  $\psi = \pm (\epsilon_{\parallel}/\epsilon_{\perp})^{1/2}/i$ ,  $\sigma$  is the conductivity of the graphene,  $t_{\text{hBN}}$  is the thickness of the hBN film, and  $\epsilon_a$  and  $\epsilon_s$  are the relative permittivities of air and the substrate, respectively. The sign of  $\psi$  is determined by the shape of the dispersion as discussed in the Supporting Information. On the other hand, outside the RS bands, the above condition is not sufficient since  $\psi$  becomes imaginary. Thus, outside the two RS bands, the modal dispersion takes the form

$$q(\omega) = \frac{1}{2} \frac{i\psi}{t_{\text{hBN}}} \ln \left[ \left( \frac{1 - i\psi(\epsilon_{\perp}/\epsilon_a) + i(q/k_0)(Z_0\sigma/\epsilon_a)}{1 + i\psi(\epsilon_{\perp}/\epsilon_a) + i(q/k_0)(Z_0\sigma/\epsilon_a)} \right) \times \left( \frac{1 - i\psi(\epsilon_{\perp}/\epsilon_s)}{1 + i\psi(\epsilon_{\perp}/\epsilon_s)} \right) \right] \quad (4)$$

In the lossless case, inside the two RS bands,  $\psi$  is real, whereas  $i\psi > 0$  outside the RS bands. It should be noted that for all subsequent calculations, we have used full-wave calculations, but we will refer to the quasistatic dispersion equations given

above for intuitive understanding (see Supporting Information for a comparison between quasistatic and full-wave results).

To understand the plasmon–phonon coupling, we consider two cases: (1) air–hBN–air (AHA) and (2) air–graphene–hBN–air (AGHA). A third case of air–graphene–hBN–graphene–air (AGHGA) has also been presented in the Supporting Information. We have chosen the geometry of symmetric waveguides (the two surrounding half-spaces are both assumed to be air) only for simpler presentation, but all our results and discussions in this section have been verified and hold true for asymmetric waveguides, which is the common situation experimentally. Later in this paper, when we do consider a substrate, these geometries will be denoted as AHS, AGHS, and AGHGS instead. The refractive index of this dummy substrate was chosen to be 1.5.

The phonon–plasmon-polariton dispersion is highlighted in the frequency range close to the two RS bands in Figures 2, panel c and 3, panel c. The nature of these modes is completely different between the in-plane (upper) and out-of-plane (lower) RS bands owing to differing types of hyperbolicity. This is described in the next two subsections. Different values of  $k_x$  on these dispersion diagrams can be experimentally accessed for instance by fabricating finite width graphene nanoribbons on top of hBN.<sup>27</sup> All the dispersion curves are represented by a intensity plot of the imaginary part of the

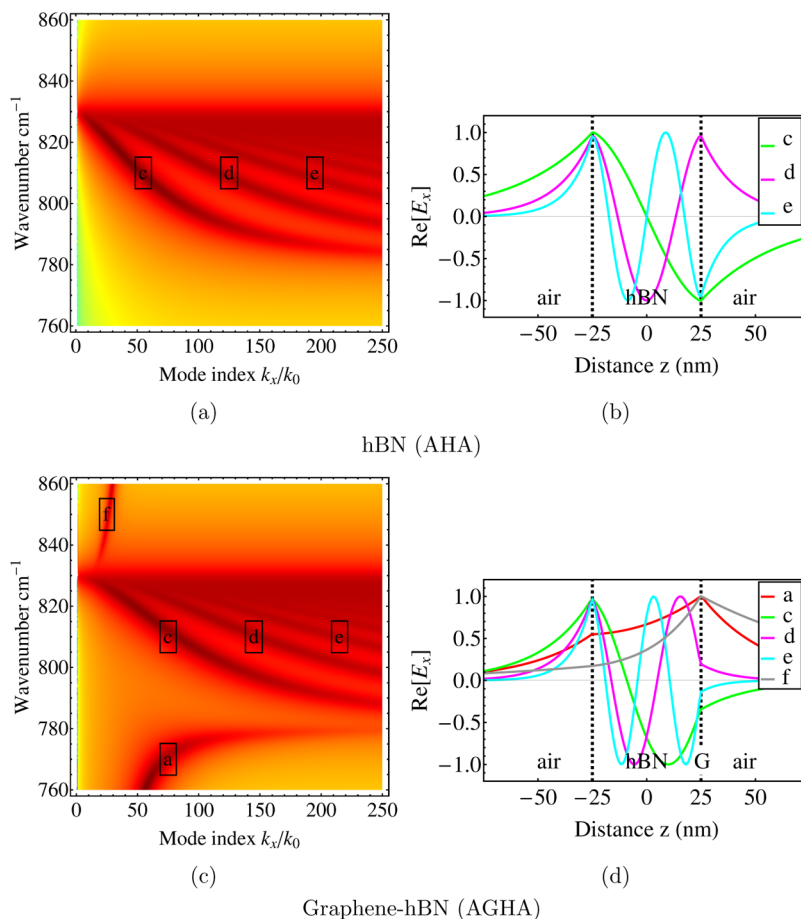


**Figure 3.** Dispersion curves and mode profiles for phonon polaritons in hBN thin slab (AHA) and coupled phonon–plasmon-polariton modes in graphene–hBN system (AGHA) near the out-of-plane (lower) RS band. Panels a–d represent the dispersion and mode profiles near the out-of-plane resonance of hBN. The alphabetical labels at different  $(k_x, \omega)$  points on each of the dispersion diagrams correspond to the field profiles on their immediate right. Thickness of hBN is  $t_{\text{hBN}} = 50$  nm, and graphene Fermi level is assumed to be 0.5 eV. Here, AHA and AGHA denote air–hBN–air and air–graphene–hBN–air, respectively.

Fresnel reflection coefficient for p-polarization in  $(\omega, k_x)$  space. The field profiles were obtained using the COMSOL MULTIPHYSICS package.

**Plasmon–Phonons for the in-Plane (Upper) RS Band.** This is the frequency range that shows type-II hyperbolicity, which means that the in-plane dielectric function is negative, and the out-of-plane component is positive. Therefore, for this band, the quantity  $\psi$  in eq 3 is less than zero also. For the AHA case, this gives several slab polariton modes for  $n = 0, 1, 2, 3, \dots$  as suggested in the dispersion in Figure 2, panel a. Each of these mode numbers corresponds to the number of nodes in the tangential electric field  $E_x$  as shown in Figure 2, panel b. It is apparent from Figure 2, panel b that the fields are mostly confined inside the hBN slab rather than the surrounding media or the interfaces, particularly for the higher order modes. It should be noted that the modes with smaller number of nodes occur at higher frequencies. This is a consequence of type-II hyperbolicity and the shape of the permittivity curve for the hBN slab.

When the top interface of the hBN slab is covered with graphene (AGHA case), we observe an interesting effect: the  $n = 0$  phonon polariton merges smoothly into a plasmon mode of the graphene,<sup>37</sup> as shown in Figure 2, panel c. Note that the phonon polariton modes inside the hBN are sinusoidal in the  $z$  direction, whereas the plasmon mode is exponentially decaying.

This is also apparent from a comparison of the field plot (Figure 2d) for frequency points labeled “a” and “c” between the AHA and the AGHA geometries where in the latter case, the field profile inside the hBN is deviating markedly from a sinusoidal profile and tending toward an exponentially decaying one. This has the additional effect of shifting the peak of the field from the bulk of hBN to the graphene.

This smooth transition is unexpected especially given the fact that at the top of this RS band, the hBN undergoes a transition<sup>46</sup> from hyperbolic to elliptical dispersion. However, since we have a thin layer of hBN, this transition becomes more gradual. This behavior can also be understood in terms of a mode coupling picture. The hybrid mode dispersion below this RS band starts becoming phonon-like as it approaches the TO frequency of the hBN. On the other hand, the lowest (zero) order phonon-polariton mode merges into the graphene plasmon mode near the LO frequency. Higher-order phonon-polariton modes are not affected by this coupling due to symmetry mismatch, which can be seen by looking at the field profiles of the modes “d” and “e” in Figure 2, panel d. The plasmon-like mode “a” does not show any node inside the hBN, whereas all the phonon-polariton modes other than “c” show one node or more. Thus, mode “c”, which is the lowest-order mode, can crossover smoothly into the plasmon. This hand

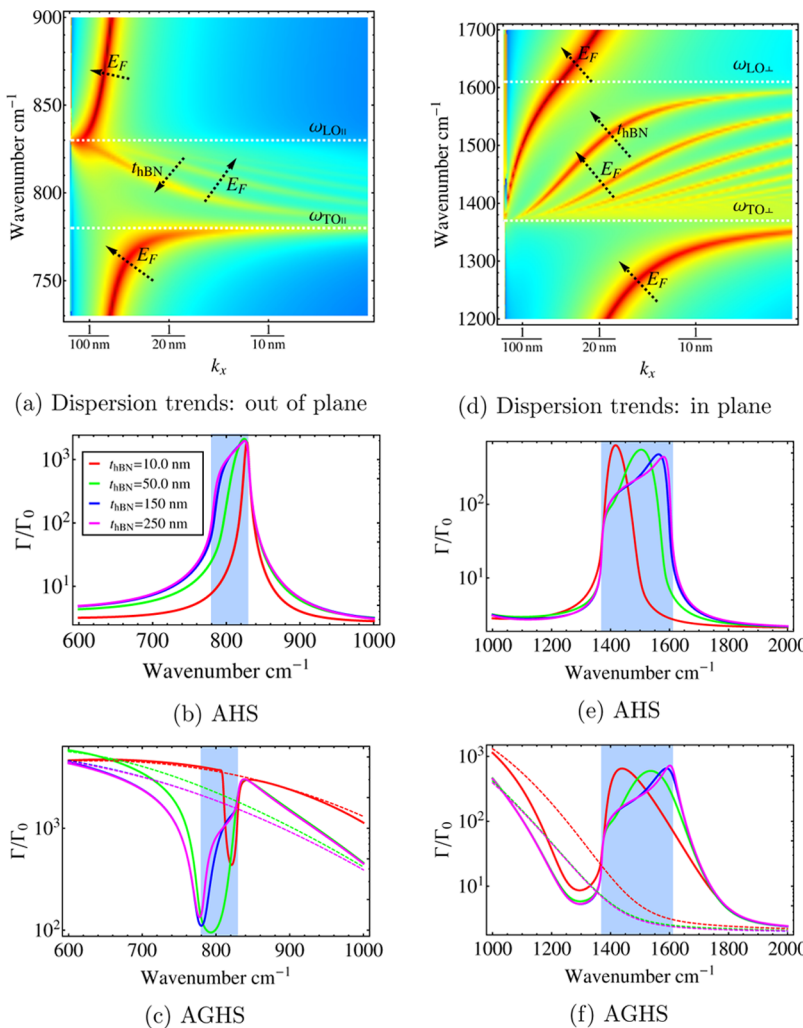


**Figure 4.** hBN thickness dependent Purcell spectra in graphene–hBN system. Panels a and d represent trends for dispersion variation as a function of hBN thickness and graphene doping near the out-of-plane and in-plane phonon resonances. We consider here the AGHS system. The arrows point in the direction of increasing  $t_{\text{hBN}}$  or  $E_F$ . The trends shown are for independent variation of the two variables and not simultaneous. Here, the x-axis is  $k_x$  represented so as to make it easier for the reader to relate it to  $1/d_s$ . See text for details. Panels b, c, e, and f represent hBN thickness dependent Purcell spectra in graphene–hBN system. Distance  $d_s$  of the quantum emitter from the hBN is fixed at 100 nm. In the AGHS case, the emitter is on the graphene side. Dashed lines show the Purcell enhancement due to graphene plasmon without the phonon-polariton contribution from the hBN slab, that is, assuming  $\epsilon_{\text{hBN}}(\omega \rightarrow 0)$ . Graphene Fermi level is assumed to be 0.5 eV.

waving argument can be rigorously substantiated by calculating the modal overlaps.

To confirm this picture, we investigated coupling to the acoustic plasmon mode<sup>47</sup> (where the tangential electric field profile has the form of a hyperbolic sine function) of the double layer graphene. This case (AGHGA) is presented in the Supporting Information. Indeed, the graphene plasmon splits into symmetric and antisymmetric modes with zero and one nodes, which merge smoothly with the zeroth- and first-order phonon-polariton modes, respectively.

**Plasmon–Phonons for the out-of-Plane (Lower) RS Band.** Phonon-polariton modes in the out-of-plane (lower) RS band for thick hBN slabs have received relatively less attention in literature so far, with the exception of ref 6, where they explored 3D resonators. This band displays type-I hyperbolicity since the out-of-plane dielectric function is negative. This difference makes its coupling to the graphene plasmon markedly different from the in-plane phonon case discussed previously.

For this band,  $\psi$  in eq 3 is positive. Thus, to make the real part of the wavevector  $q$  positive, we need  $n < 0$ . This is also reflected in the field plots in Figure 3, panel b where it is observed that there is no mode with zero number of nodes. In other words, the minimum value of  $|n|$  is 1 instead of zero. A simple explanation of this behavior can be obtained by reference to the relative signs of the Poynting vector and the wave-vector.<sup>48</sup> In the case of out-of-plane resonance, since the dispersion is type-I, the Poynting vector component  $S_z$  and the wavevector component  $k_z$  point in the same direction. Thus, the dispersion equation  $k_z t_{\text{hBN}} + \phi_r = n\pi$  does not admit  $n = 0$  solution since the left-hand side is strictly positive. On the other hand, for the in-plane (upper) mode, type-II dispersion causes  $S_z$  and  $k_z$  to point in opposite directions, which permits the left side approach zero value, thus allowing  $n = 0$  solution. Such behavior also consistent with the predictions in the literature.<sup>48</sup>

In this case, one can observe that the ordering of the modes in the out-of-plane or lower RS band is such that that the lower-order mode occurs at smaller frequency, unlike the case of in-plane (upper) RS band. Again, this is due to the difference in

the type of hyperbolicity. This trend is consistent with the findings in the literature.<sup>5,49</sup>

In the AGHA case, it is observed that below the RS band, the hybridized mode becomes phonon-like as it approaches the TO phonon frequency. The hybridized mode branch on the top of the RS band acquires a phonon-polariton character near  $\omega_{LO}$ . We also observe the effect of mode repulsion, which causes the first-order phonon polariton to blueshift compared to the case without graphene. As shown in the Supporting Information, this behavior persists for the AGHGA case where both the graphene plasmon modes couple with the phonon polaritons to form hybridized modes, which acquire phonon-polariton-like character near  $\omega_{LO}$  and  $\omega_{TO}$ .

In summary, we observe that the coupling between the graphene plasmon and the hBN phonon polaritons is completely different between the two RS bands. This is attributable to the different types of hyperbolicity associated with the in-plane (upper) and the out-of-plane (lower) phonon modes. In the next section, we will attempt to use this coupling for tuning the local density of states.

**Tunable Spectral Dips in Emission.** When an excited quantum emitter is placed near a material system that can support a photonic mode, its lifetime is modified compared to the case when it emits in free space. This phenomenon is called Purcell effect.<sup>50</sup> The emitter can typically be an excited atom, molecule, or quantum dot.

The emitter can release its excitation energy into free space radiative modes as well as resonant modes and nonradiative or lossy modes of the material. The radiative contribution is modified due to the change of the boundary conditions for the electromagnetic fields because of the presence of the material. This results in the modification of far-field emission patterns.<sup>51</sup>

More interestingly, the emitter can also release its energy through the available resonant modes in the neighboring matter. The strength of this light-matter interaction is governed by the ratio of quality factor and the volume of the available photonic mode. The basic idea of nanophotonics is to provide subwavelength mode volumes, which enhance this interaction. For instance, the power of graphene plasmonics is in providing very small mode volumes.<sup>19</sup> On the other hand, hBN phonon polaritons provide, in addition, high quality factors as well.<sup>5,6</sup> The latter is due to intrinsically long-lived phonon polaritons and has also been observed in other dielectrics such as SiC.<sup>52,53</sup>

One key aspect of hyperbolic materials is that when moving from a hyperbolic dispersion regime to an elliptical one, a sharp change in the local density of states (LDOS) is observed.<sup>46</sup> This is due to the availability of high-k states in the hyperbolic band. To explore this phenomenon in the context of graphene–hBN slab system, we considered the spontaneous emission enhancement (Purcell effect) of a quantum emitter with polarization perpendicular ( $\hat{z}$ ) to the hBN surface. While the phonon-polariton modes in hBN are purely transverse magnetic (TM), there exists the possibility of transverse electric (TE) guided modes in hBN (particularly in the region where it has elliptical dispersion) and also TE plasmons in graphene.<sup>54</sup> Therefore, in this work, for simplicity the orientation of the emitter was chosen to be  $\hat{z}$  since the  $\hat{z}$ -dipole moment will only couple to the TM modes. However, parallel polarization can also be treated in a similar manner. In the present case, the spontaneous emission rate of the  $\hat{z}$ -polarized dipole, also called the partial LDOS or PLDOS, is given by<sup>46,55</sup>

$$\frac{\Gamma}{\Gamma_0} = 1 + \frac{3}{2k_0^3} \int_0^\infty dk_x k_x \Re \left\{ \frac{k_x^2 e^{2ik_z d_s} r_p(\omega, k_x)}{k_z} \right\} \quad (5)$$

where  $\Gamma_0$  is the free space radiative decay rate,  $d_s$  is the distance of the quantum emitter (source) from the hBN slab, and  $r_p(\omega, k_x)$  is the Fresnel reflection coefficient from the graphene-coated hBN slab. This expression includes both radiative as well as nonradiative contributions to the total decay rate. The Purcell enhancement in the hyperbolic regime is clearly observable in the AHS case shown in Figure 4, panels b and e, where the PLDOS rises sharply inside both the RS bands. As shown in the following, in the presence of graphene, a dip in the Purcell enhancement is observed, whose spectral width and location are strongly tunable both actively using electrostatic doping and also by changing the thickness of hBN. In particular, for the out-of-plane (lower) RS band, the reduction in the decay rate is consistently found to be about an order of magnitude in the presence of phonon–plasmon coupling. The observed dips in Purcell spectrum are due to coupling between spectrally broad plasmon and much narrower phonon resonance. Such dips are analogous to induced transparency in the absorption spectrum observed recently in such systems.<sup>56</sup> The induced transparency can be understood in the classical coupled oscillator picture with oscillators of contrasting damping rate.<sup>38,56</sup> Such a large modification in the PLDOS suggests possible application in tuning the energy transfer to hBN via guided phonon-polariton modes. Note that the presence of graphene is also expected to enhance the nonradiative decay rate of the emitter via energy transfer into the electron–hole pairs and the plasmon mode.<sup>19</sup>

In the next two subsections, we will describe two approaches to tuning the Purcell spectra: via hBN thickness and active tuning using electrostatic doping of graphene. We want to remark here that the spectrum does depend on the emitter location. In particular, the contrast of the spectral dip depends strongly on the emitter location. A detailed study about the emitter location dependence is discussed in the Supporting Information. In the following, we choose a fixed emitter distance of 100 nm from the graphene for demonstration purposes.

**Purcell Spectra versus hBN Thickness.** The dispersion of guided modes in the hBN slab depends strongly on its thickness. This variation in the dispersion has a strong influence on the PLDOS spectra. Let us focus on the AHS out-of-plane phonon case first. In this case, as shown in Figure 4, panel a, with increase in hBN thickness  $t_{hBN}$ , the phonon-polariton dispersion moves closer to  $\omega_{TO}$  or the lower end of the RS band at small  $k_x$ . The implication of this movement is that the PLDOS peak starts moving from the upper end of the RS band (at small  $t_{hBN}$ ), broadening toward the lower end (at large  $t_{hBN}$ ). The broadening occurs again because as  $t_{hBN}$  is increased, (1) more states are available throughout the RS band (at fixed  $k_x$ ), and (2) the red-shifted phonon polaritons, especially at low  $k_x$ , have greater curvature (more dispersive rather than flat). Both of these expectations are verified in the calculations shown in Figure 4, panel b.

With the graphene coating on the hBN slab, spectral dips of an order of magnitude can be obtained in the PLDOS. Let us try to understand what happens when we enter the RS band from below  $\omega_{TO}$ . If we are at sufficiently large emitter distance  $d_s$  (corresponding to maximal PLDOS contribution coming from low  $k_x \approx 1/d_s$ ), as discussed in the Supporting

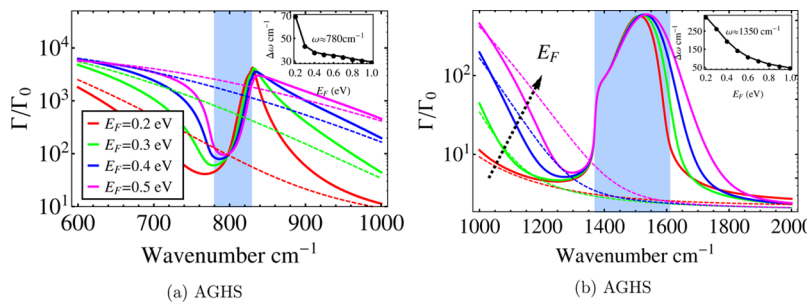


**Figure 5.** Fermi level dependent Purcell spectra in graphene–hBN system. The doping of the graphene is varied. The thickness of the hBN slab is 50 nm. Distance  $d_s$  of the quantum emitter from the hBN is fixed at 100 nm. The AGHS case has been considered with the emitter on the air side. Panel a represents Purcell spectra around out-of-plane (lower) resonance, and panel b represents that near in-plane (upper) resonance. Dashed lines show the Purcell enhancement due to graphene plasmon without the phonon-polariton contribution from the hBN slab, that is, assuming  $\epsilon_{\text{hBN}}(\omega \rightarrow 0)$ . The insets in both the panels represent the full width at half maxima of the dips as a function of the graphene Fermi level.

Information), the plasmon-like hybrid mode branch is far below  $\omega_{\text{TO}}$  and its curvature implies that it will contribute a broad peak located far below  $\omega_{\text{TO}}$ . Inside the RS band on the other hand, the lowly dispersive phonon modes are available. As a result, there is a frequency range where there is no apparent polariton mode, that is, a spectral gap exists. This is the origin of the spectral dips.

As  $t_{\text{hBN}}$  increases, the width of the dip becomes narrow because it is “pushed” from the right by the phonon-polariton states, which are being red-shifted, as shown in Figure 4, panel a. This explains the movement of the spectral dip in Figure 4, panel c.

This behavior persists for the in-plane modes as shown in Figure 4, panels e and f, with the difference being the opposite trend of peak movements, on account of differing types of hyperbolicity, as explained earlier.

**Active Control of Spectral Dips.** The Fermi level of graphene can be tuned via electrostatic doping.<sup>57</sup> This is one of the main motivations for using graphene for photonics applications.<sup>25,58</sup> Importantly, graphene with higher doping has a plasmon dispersion, which is closer to the light line.<sup>19,24,59</sup> Thus, for a fixed dipole distance and hBN thickness, changing the Fermi level offers a route for active control of the spectral location and width of the spectral dips in PLDOS.

To demonstrate such a gate tunability of the PLDOS, we carried out calculations for the AGHS case as shown in Figure 5. For the out-of-plane case, we expect that at larger doping (or larger  $E_F$ ), the graphene plasmon-like branch below  $\omega_{\text{TO}}$  will flatten out at smaller  $k_x$ , as shown in Figure 4, panel a. Conversely, at a fixed value of emitter distance  $d_s$ , this graphene plasmon-like branch will have more curvature (i.e., more dispersive as opposed to being flat) and will be farther below  $\omega_{\text{TO}}$  for smaller doping. On the other hand, because of availability of states inside the RS band, the PLDOS is expected to rise there. This results in a dip occurring between the two peaks near  $\omega_{\text{TO}}$ . Moreover, as the graphene doping increases, this PLDOS dip is expected to become sharper because it is “pushed” by the blue-shifting plasmon-like branch.

Second, toward the upper end of this (out-of-plane or lower) RS band, we observe an interesting trend. The half line width of the part of PLDOS peak, which is inside the RS band, decreases with increasing  $E_F$ . On the other hand, the line width of the PLDOS peak outside the RS band (at the higher frequency end) increases with increasing  $E_F$ . There are two effects at play here. First, for smaller Fermi-level, since the graphene plasmon is highly confined close to the graphene, it does not interact

very strongly with the phonon polariton since the field overlap between the two is smaller. As the doping is increased, the plasmon confinement decreases, and as shown in Figure 4, panel a, the phonon polaritons inside the RS are repelled. Second, at reasonably small  $k_x$ , not only does this repulsion cause a blue-shift of the phonon polaritons, but also makes them less dispersive, resulting in narrower line width inside the RS band at high graphene doping. On the other hand, outside the RS band for frequencies above  $\omega_{\text{LO}}$ , the hybrid mode is flatter for smaller doping. This causes the line widths of the PLDOS peaks to the right of  $\omega_{\text{LO}}$  to broaden as doping is increased. A subtle point to note here is that the graphene damping is expected to decrease with increasing  $E_F$  since we assumed the relaxation time  $\tau$  to be proportional to  $E_F$ . We have also checked that these trends persist for the case of constant  $\tau$ .

Similar but complementary trends are observed for the in-plane (upper) modes as shown in Figure 5, panel b. Note that because of high frequency, the interband excitations begin to damp the graphene plasmon mode, which results in an overall decrease in the PLDOS of the uncoupled graphene itself. Interestingly, for the in-plane (upper) band, the spontaneous emission rate is very sensitive to graphene doping near  $\omega_{\text{LO}}$  ( $1610 \text{ cm}^{-1}$ ). Near  $\omega_{\text{LO}}$ , we observe that as we go from higher to lower doping, the decay rate becomes smaller. This trend can be explained as before, using Figure 4, panel d. In accordance with Figure 4, panel d, with decreasing  $E_F$ , the phonon polariton plasmon modes redshift, resulting in lowering of the decay rate at this frequency (note that we have to look at constant  $k_x = 1/d_s$ ). If we further decrease the Fermi level, we observe (not shown) that beyond a critical point, the decay rate rises again. This is because at lower doping, the electron–hole pair emission channel opens up in graphene.<sup>60</sup> On the other hand, further inside this RS band at lower frequencies, the decay rate is almost independent of the graphene Fermi level.

We have further presented the full width at half minimum (fwhm) of the two spectral dips, as a function of graphene Fermi level in the insets of Figure 5. We note here that the fwhm values can reach quite small values for higher doping. For instance, near the  $\omega_{\text{TO}}$  of both the RS bands, the dips have  $\omega/\Delta\omega \approx 30$  for a doping level of  $E_F = 1 \text{ eV}$ . Higher values of  $\omega/\Delta\omega$  for these dips could be achieved by optimizing the hBN thickness, graphene doping, and the emitter location.

The above analysis raises a further question about the relative contributions to emission. The emission can be split into three broad contributions:

- (1) Radiative: For our chosen material and geometrical parameters, the radiative contribution is too small compared to the other two routes mentioned below.
- (2) Hybrid plasmon–phonon modes: Depending on the frequency, these hybrid modes can resemble plasmon polaritons, phonon polaritons, or both. In the presence of material loss, it is actually hard to distinguish this contribution from the nonradiative terms. To remedy this, we choose the limit where all the material loss is set to zero and consider the contribution to the LDOS from the poles of the Fresnel reflection coefficient. This approach is also consistent with that in the literature.<sup>61</sup>
- (3) Nonradiative modes: This is the contribution remaining after subtracting the pole contribution to the LDOS from the total LDOS.

Relative contributions of these emission pathways are presented in the Supporting Information. We observe that near the location of the two spectral dips, the contribution to spontaneous emission from the plasmon–phonon poles is largely suppressed. Away from the dips, however, the emission is dominated by the pole contribution from the plasmon–phonon mode. At higher frequency, specifically for  $\hbar\omega > E_F$ , the interband damping tends to dominate the emission spectrum instead.

**Conclusion and Outlook.** In this work, we have shown that heterostructures composed of graphene and hBN can provide a highly versatile tool for controlling light matter interaction at the nanoscale. The gate tunability of graphene plasmons can be combined with the high confinement property of hBN phonon polaritons, allowing for new metamaterials that marry the unique qualities of the two. Being a hyperbolic material, the hBN provides two completely different regimes of plasmon–phonon coupling in the presence of graphene. The spectral dips in spontaneous emission enhancement are an example of this coupling. The width of the spectral dip can be controlled by adjusting the Fermi level of graphene and the thickness of the hBN. This can provide a powerful route to tunable emission rate, both passive and dynamic. In particular, this could find application in vibrational spectroscopy<sup>62</sup> and stimulated Raman scattering, with the Purcell dip near  $\omega_{TO}$  of either RS band effectively being used as a gate tunable notch filter. Our findings might find applications in photodetection,<sup>63</sup> electrically tunable thermal management via broadband near-field heat transfer,<sup>64</sup> and subwavelength imaging.<sup>65,66</sup> The analysis and general principles presented in this paper apply equally well to other systems of hyperbolic materials, both natural<sup>67</sup> and artificial.<sup>33</sup>

After the submission of our paper, a related experimental demonstration of tunable phonon-polariton modes in the graphene–hBN system was brought to our attention.<sup>68</sup>

## ■ ASSOCIATED CONTENT

### Supporting Information

Detailed theoretical calculation method, dependence of Purcell spectra on various other combinations of graphene Fermi level, hBN thickness, and distance of the emitter from the graphene. This material is available free of charge via the Internet at <http://pubs.acs.org>.

## ■ AUTHOR INFORMATION

### Corresponding Author

\*E-mail: nicfang@mit.edu.

## Notes

The authors declare no competing financial interest.

## ■ ACKNOWLEDGMENTS

A.K. and N.X.F. acknowledge the financial support by the National Science Foundation (NSF) (Grant No. CMMI-1120724) and Air Force Office of Scientific Research Multidisciplinary University Research Initiative (AFOSR MURI) (Award No. FA9550-12-1-0488). T.L. acknowledges support from University of Minnesota. K.H.F. acknowledges financial support from Hong Kong RGC Grant No. 509813. A.K. acknowledges helpful comments from Prof. Marin Soljačić at MIT.

## ■ REFERENCES

- (1) Maier, S. A. *Plasmonics: Fundamentals and Applications*; Springer: New York, 2007.
- (2) Ozbay, E. *Science* **2006**, *311*, 189–193.
- (3) Barnes, W. L.; Dereux, A.; Ebbesen, T. W. *Nature* **2003**, *424*, 824–830.
- (4) Huber, A. J.; Deutsch, B.; Novotny, L.; Hillenbrand, R. *Appl. Phys. Lett.* **2008**, *92*, 203104.
- (5) Dai, S.; Fei, Z.; Ma, Q.; Rodin, A. S.; Wagner, M.; McLeod, A. S.; Liu, M. K.; Gannett, W.; Regan, W.; Watanabe, K.; et al. *Science* **2014**, *343*, 1125–1129.
- (6) Caldwell, J. D.; Kretinin, A. V.; Chen, Y.; Giannini, V.; Fogler, M. M.; Francescato, Y.; Ellis, C. T.; Tischler, J. G.; Woods, C. R.; Giles, A. J. *Nat. Commun.* **2014**, *5*, No. 5221.
- (7) Hillenbrand, R.; Taubner, T.; Keilmann, F. *Nature* **2002**, *418*, 159–162.
- (8) Greffet, J.-J.; Carminati, R.; Joulain, K.; Mulet, J.-P.; Mainguy, S.; Chen, Y. *Nature* **2002**, *416*, 61–64.
- (9) Xu, X. G.; Ghamsari, B. G.; Jiang, J.-H.; Gilburd, L.; Andreev, G. O.; Zhi, C.; Bando, Y.; Golberg, D.; Berini, P.; Walker, G. C. *Nat. Commun.* **2014**, *5*, No. 4782.
- (10) Jacob, Z. *Nat. Mater.* **2014**, *13*, 1081–1083.
- (11) Fang, N.; Lee, H.; Sun, C.; Zhang, X. *Science* **2005**, *308*, 534–537.
- (12) Estevâm da Silva, R.; Macêdo, R.; Dumelow, T.; da Costa, J.; Honorato, S.; Ayala, A. *Phys. Rev. B* **2012**, *86*, 155152.
- (13) Kneipp, K.; Wang, Y.; Kneipp, H.; Perelman, L.; Itzkan, I.; Dasari, R.; Feld, M. *Phys. Rev. Lett.* **1997**, *78*, 1667–1670.
- (14) Talley, C. E.; Jackson, J. B.; Oubre, C.; Grady, N. K.; Hollars, C. W.; Lane, S. M.; Huser, T. R.; Nordlander, P.; Halas, N. J. *Nano Lett.* **2005**, *5*, 1569–1574.
- (15) Christensen, J.; Manjavacas, A.; Thongrattanasiri, S.; Koppens, F. H. L.; García de Abajo, F. J. *ACS Nano* **2012**, *6*, 431–440.
- (16) Atwater, H. A.; Polman, A. *Nat. Mater.* **2010**, *9*, 205–213.
- (17) Chang, D.; Sørensen, A.; Hemmer, P.; Lukin, M. *Phys. Rev. Lett.* **2006**, *97*, 053002.
- (18) Gonzalez-Tudela, A.; Martin-Cano, D.; Moreno, E.; Martin-Moreno, L.; Tejedor, C.; Garcia-Vidal, F. *Phys. Rev. Lett.* **2011**, *106*, 020501.
- (19) Koppens, F. H. L.; Chang, D. E.; Garcia de Abajo, F. J. *Nano Lett.* **2011**, *11*, 3370–3377.
- (20) Stroscio, M. A.; Dutta, M. *Phonons in Nanostructures*; Cambridge University Press: Cambridge, UK, 2001.
- (21) Kliewer, K. L.; Fuchs, R. *Phys. Rev.* **1966**, *144*, 495–503.
- (22) Mills, D. L.; Chen, Y. J.; Burstein, E. *Phys. Rev. B* **1976**, *13*, 4419–4438.
- (23) Subbaswamy, K.; Mills, D. *Solid State Commun.* **1978**, *27*, 1085–1088.
- (24) Low, T.; Avouris, P. *ACS Nano* **2014**, *8*, 1086–1101.
- (25) Ju, L.; Geng, B.; Horng, J.; Girit, C.; Martin, M.; Hao, Z.; Bechtel, H. A.; Liang, X.; Zettl, A.; Shen, Y. R.; et al. *Nat. Nanotechnol.* **2011**, *6*, 630–634.

- (26) Grigorenko, A. N.; Polini, M.; Novoselov, K. S. *Nat. Photonics* **2012**, *6*, 749–758.
- (27) Yan, H.; Low, T.; Zhu, W.; Wu, Y.; Freitag, M.; Li, X.; Guinea, F.; Avouris, P.; Xia, F. *Nat. Photonics* **2013**, *7*, 394–399.
- (28) Chen, J.; Badioli, M.; Alonso-González, P.; Thongrattanasiri, S.; Huth, F.; Osmond, J.; Spasenović, M.; Centeno, A.; Pesquera, A.; Godignon, P.; et al. *Nature* **2012**, *487*, 77–81.
- (29) Fei, Z.; Rodin, A. S.; Andreev, G. O.; Bao, W.; McLeod, A. S.; Wagner, M.; Zhang, L. M.; Zhao, Z.; Thiemens, M.; Dominguez, G.; et al. *Nature* **2012**, *487*, 82–85.
- (30) Jablan, M.; Buljan, H.; Soljačić, M. *Phys. Rev. B* **2009**, *80*, 245435.
- (31) Poddubny, A.; Iorsh, I.; Belov, P.; Kivshar, Y. *Nat. Photonics* **2013**, *7*, 948–957.
- (32) Jacob, Z.; Smolyaninov, I. I.; Narimanov, E. E. *Appl. Phys. Lett.* **2012**, *100*, No. 1204.
- (33) Yu Guo, W. N.; Cortes, C. L.; Jacob, Z. *Adv. Optoelectron.* **2012**, *2012*, No. 452502.
- (34) Belov, P. A. *Microwave Opt. Technol. Lett.* **2003**, *37*, 259–263.
- (35) Guo, Y.; Cortes, C. L.; Molesky, S.; Jacob, Z. *Appl. Phys. Lett.* **2012**, *101*, No. 131106.
- (36) Dean, C. R.; Young, A. F.; Meric, I.; Lee, C.; Wang, L.; Sorgenfrei, S.; Watanabe, K.; Taniguchi, T.; Kim, P.; Shepard, K. L.; et al. *Nat. Nanotechnol.* **2010**, *5*, 722–726.
- (37) Woessner, A.; Lundeberg, M. B.; Gao, Y.; Principi, A.; Alonso-González, P.; Carrega, M.; Watanabe, K.; Taniguchi, T.; Vignale, G.; Polini, M.; et al. *Nat. Mater.* **2014**, *14*, 421–425.
- (38) Yan, H.; Low, T.; Guinea, F.; Xia, F.; Avouris, P. *Nano Lett.* **2014**, *14*, 4581–4586.
- (39) Brar, V. W.; Jang, M. S.; Sherrott, M.; Kim, S.; Lopez, J. J.; Kim, L. B.; Choi, M.; Atwater, H. *Nano Lett.* **2014**, *14*, 3876–3880.
- (40) Song, L.; Ci, L.; Lu, H.; Sorokin, P. B.; Jin, C.; Ni, J.; Kvashnin, A. G.; Kvashnin, D. G.; Lou, J.; Yakobson, B. I. *Nano Lett.* **2010**, *10*, 3209–3215.
- (41) Reina, A.; Jia, X.; Ho, J.; Nezich, D.; Son, H.; Bulovic, V.; Dresselhaus, M. S.; Kong, J. *Nano Lett.* **2009**, *9*, 30–35.
- (42) Cai, Y.; Zhang, L.; Zeng, Q.; Cheng, L.; Xu, Y. *Solid State Commun.* **2007**, *141*, 262–266.
- (43) Falkovsky, L. A.; Varlamov, A. A. *Eur. Phys. J. B* **2007**, *56*, 281–284.
- (44) Jablan, M.; Soljacic, M.; Buljan, H. *Conf. Proc. IEEE* **2013**, *101*, 1689–1704.
- (45) Bolotin, K.; Sikes, K.; Jiang, Z.; Klime, M.; Fudenberg, G.; Hone, J.; Kim, P.; Stormer, H. *Solid State Commun.* **2008**, *146*, 351–355.
- (46) Krishnamoorthy, H. N. S.; Jacob, Z.; Narimanov, E.; Kretzschmar, I.; Menon, V. M. *Science* **2012**, *336*, 205–209.
- (47) Hwang, E. H.; das Sarma, S. *Phys. Rev. B* **2009**, *80*, 205405.
- (48) Huang, Z.; Narimanov, E. E. *Opt. Express* **2013**, *21*, 15020–15025.
- (49) Yang, X.; Yao, J.; Rho, J.; Yin, X.; Zhang, X. *Nat. Photonics* **2012**, *6*, 450–453.
- (50) Purcell, E. M. *Phys. Rev.* **1946**, *69*, 681.
- (51) Ford, G.; Weber, W. *Phys. Rep.* **1984**, *113*, 195–287.
- (52) Wang, T.; Li, P.; Hauer, B.; Chigrin, D. N.; Taubner, T. *Nano Lett.* **2013**, *13*, 5051–5055.
- (53) Caldwell, J. D.; Glembotck, O. J.; Francescato, Y.; Sharac, N.; Giannini, V.; Bezires, F. J.; Long, J. P.; Owrutsky, J. C.; Vurgaftman, I.; Tischler, J. G. *Nano Lett.* **2013**, *13*, 3690–3697.
- (54) Mikhailov, S. A.; Ziegler, K. *Phys. Rev. Lett.* **2007**, *99*, 016803.
- (55) Cortes, C. L.; Newman, W.; Molesky, S.; Jacob, Z. *J. Opt.* **2012**, *14*, 063001.
- (56) Low, T.; Guinea, F.; Yan, H.; Xia, F.; Avouris, P. *Phys. Rev. Lett.* **2014**, *112*, 116801.
- (57) Novoselov, K. S.; Geim, A. K.; Morozov, S. V.; Jiang, D.; Zhang, Y.; Dubonos, S. V.; Grigorieva, I. V.; Firsov, A. A. *Science* **2004**, *306*, 666–669.
- (58) Koppens, F. H. L.; Mueller, T.; Avouris, P.; Ferrari, A. C.; Vitiello, M. S.; Polini, M. *Nat. Nanotechnol.* **2014**, *9*, 780–793.
- (59) Yao, Y.; Kats, M. A.; Genevet, P.; Yu, N.; Song, Y.; Kong, J.; Capasso, F. *Nano Lett.* **2013**, *13*, 1257–1264.
- (60) Tielrooij, K. J.; Orona, L.; Badioli, A. F.; Navickaitė, M.; Coop, G.; Nanot, S.; Kalinic, S.; Cesca, B.; Gaudreau, T.; Ma, Q.; et al. *Nat. Phys.* **2015**, *11*, 281–287.
- (61) Chang, D. E.; Sørensen, A. S.; Hemmer, P. R.; Lukin, M. D. *Phys. Rev. B* **2007**, *76*, 035420.
- (62) Li, Y.; Yan, H.; Farmer, D. B.; Meng, X.; Zhu, W.; Osgood, R. M.; Heinz, T. F.; Avouris, P. *Nano Lett.* **2014**, *14*, 1573–1577.
- (63) Freitag, M.; Low, T.; Zhu, W.; Yan, H.; Xia, F.; Avouris, P. *Nat. Commun.* **2013**, *4*, No. 1951.
- (64) Liu, X.; Zhang, R. Z.; Zhang, Z. *ACS Photonics* **2014**, *1*, 785–789.
- (65) Li, P.; Taubner, T. *ACS Nano* **2012**, *6*, 10107–10114.
- (66) Taubner, T.; Korobkin, D.; Urzhumov, Y.; Shvets, G.; Hillenbrand, R. *Science* **2006**, *313*, 1595.
- (67) Alekseyev, L. V.; Podolskiy, V. A.; Narimanov, E. E. *Adv. Optoelectron.* **2012**, *2012*, No. 267564.
- (68) Dai, S.; Ma, Q.; Zhu, S.-E.; Liu, M. K.; Andersen, T.; Fei, Z.; Goldflam, M.; Wagner, M.; Watanabe, K.; Taniguchi, T. et al. *arXiv:* 1501.06956 1501, 2015.